Probing the $^{17}F + p$ potential by elastic scattering at near-barrier energies

N. Patronis,[1,*] A. Pakou,[1] D. Pierroutsakou,[2] A. M. Sánchez-Benítez,[3] L. Acosta,[3,4] N. Alamanos,[5] A. Boiano,[2] G. Inglima,[6] D. Filipescu,[7] T. Glodariu,[7] A. Guglielmetti,[8] M. La Commara,[6] G. Lalazissis,[9] I. Martel,[3] C. Mazzocchi,[8] M. Mazzocco,[10] P. Molini,[10] C. Parascandolo,[2] M. Sandoli,[6] C. Signorini,[10] R. Silvestri,[6] F. Soramel,[10] E. Stiliaris,[11] M. Romoli,[2] A. Trzcinska,[12] K. Zerva,[1] E. Vardaci,[6] and A. Vitturi[10]

[1]*Department of Physics and HINP, The University of Ioannina, GR-45110 Ioannina, Greece*
[2]*INFN–Sezione di Napoli, via Cintia, I-80125 Napoli, Italy*
[3]*Departamento de Física Aplicada, Universidad de Huelva E-21071 Huelva, Spain*
[4]*Laboratori Nazionali del Sud–INFN, Via S. Sofia 62, I-95123 Catania, Italy*
[5]*CEA-Saclay, DAPNIA-SPhN, Gif-sur-Yvette, France*
[6]*Dipartimento di Scienze Fisiche, Università di Napoli "Federico II", and INFN–Sezione di Napoli, via Cintia, I-80125 Napoli, Italy*
[7]*"Horia Hulubei" National Institute of Physics and Nuclear Engineering, Bucharest, Romania*
[8]*Universita' degli Studi di Milano and INFN–Sezione di Milano, via Celoria 16, I-20133 Milano, Italy*
[9]*Department of Theoretical Physics, Aristotle University of Thessaloniki, GR-54124 Thessaloniki, Greece*
[10]*Dipartimento di Fisica and INFN–Sezione di Padova, via F. Marzolo 8, I-35131 Padova, Italy*
[11]*Institute of Accelerating Systems and Applications and Department of Physics, University of Athens, Athens, Greece*
[12]*Heavy Ion Laboratory, University of Warsaw, Pasteura 5a, 02-093 Warsaw, Poland*

(Received 18 November 2011; published 14 February 2012)

Proton elastic scattering angular distributions for the reaction $^{17}F + p$, were measured in inverse kinematics over a wide angular range ($\theta_{c.m.} = 50^\circ$–160°) at two near-barrier energies of 3.5 and 4.3 MeV/u. The optical potential was probed in a phenomenological and microscopic approach. Moreover, total reaction cross-sections were also determined via optical potential analysis and were used as a signature for probing a possible halo structure of this proton-rich nucleus.

DOI: 10.1103/PhysRevC.85.024609 PACS number(s): 25.40.Cm, 25.60.Bx, 25.70.Bc, 27.20.+n

I. INTRODUCTION

The study of both neutron- and proton-rich drip-line nuclei is at the forefront of nuclear physics research today. The development of a neutron (proton) halo or skin leads to a revision of our views on standard models of the nuclear structure and our views on optical potential and reaction mechanisms. Since several of these nuclei play a major role in the evolution of the Universe, their study is very appealing. In astrophysics, the determination of low-energy cross sections, which belong to a deep sub-barrier region, is a difficult task, both from theoretical and experimental points of view, and the possible approach relies on extrapolations. Weakly bound projectiles exhibit a pronounced cluster structure with a very small binding energy, and they present low-density excited states up to several MeV. Under these conditions, the choice of a standard optical potential may be inapplicable. Therefore, in principle, elastic scattering and induced reaction measurements at low energies could be very useful.

Proton-nucleus elastic scattering has been traditionally used to probe the nuclear potential. In this respect, extensive studies have been performed and both phenomenological and microscopic potential models have been developed [1–11]. Concerning stable projectiles, a large amount of experimental data has been successfully interpreted through such models with the adjustment of only a few parameters [3,5,6,12–19]. A few studies were also devoted to radioactive nuclei at energies above $E = 10$ MeV/u [20–22]. In this respect it is of prime importance to probe the potential for drip-line nuclei in a broad energy region, especially when they are involved in nuclear reactions of astrophysical interest.

Indeed this is the case for ^{17}F. The nucleus ^{17}F is a very important drip-line nucleus involved in reactions of x-ray burster scenarios, such as $^{14}O(\alpha, p)^{17}F$ (see, e.g., Ref. [23]), $^{17}F(p, \gamma)^{18}Ne$ (see, e.g., Ref. [24]), and $^{16}O(p, \gamma)^{17}F$ (e.g., Ref. [25]). As a proton-rich nucleus, with binding energy of the last proton for the ground state $S_p = 600$ keV and the first excited one $S_p = 105.13$ keV, it is expected to possess an unusual structure of a proton halo or a proton skin, with strong implications in nuclear reaction mechanisms. The importance of this exotic structure is underlined in Ref. [25]. A possible proton exotic structure for the ground state ($I = 5/2^+$) and first excited state has been investigated both experimentally and theoretically [25–34]. The obtained results, although occasionally controversial, give the impressions of a proton-skin ground state and a proton-halo first excited state. It should be noted that the observation of a proton halo or skin is a difficult task. Despite the active investigation of proton-rich nuclei, we are not very close to a thorough understanding of the properties or even the existence of a proton halo. Major difficulties can be attributed to the Coulomb interaction between the protons of the halo and the target, which may distort the implied proton halo structure. It is therefore necessary to distinguish between the role of reaction dynamics and the role of an extended proton density distribution. In this connection there are two types of targets to be used: either very heavy targets, in order

*npatronis@uoi.gr

to obtain the largest contribution of interaction dynamics, or very light targets in order to avoid the Coulomb distortion. For this purpose neutron targets could have been the ideal solution, the absence of which leads to the choice of a "simple" target such as ^{1}H. This view is generally supported when microscopic calculations are undertaken for probing the nucleus structure. In this case density distributions of only one of the encounters will be taken into account, facilitating the solution of the problem.

In the above context, we present in this work elastic scattering angular distributions of $p(^{17}\mathrm{F}, p)$, in a wide angular range ($\theta_{\mathrm{c.m.}} = 50^{\circ}$–$160^{\circ}$) at two near-barrier energies, namely $E_{^{17}\mathrm{F}} = 3.5$ and 4.3 MeV/u, a very interesting energy region from the astrophysical point of view [23]. Excitation functions are reported by Harss *et al.* [23] only at particular angles from 3.23 to 4.12 MeV/u beam energy and were used for normalization purposes. The results are considered in a macroscopic as well as in a microscopic theoretical context with the aim of probing the potential, and to verify if a neutron-deficient drip-line nucleus such as ^{17}F follows the systematic behavior determined for stable nuclei.

The macroscopic calculations were performed with the code ECIS [35], and various standard global parametrizations for the potential, namely the Becchetti-Greenlees [3] and Varner-CH89 [4], were used. Other parametrizations more suitable to the mass number and energy range, e.g., those of Watson [7] and Xiaohua [11], were also used. Subsequently some of the parameters of the global potentials were fitted to the data and finally, from a free parameter search, a couple of improved sets of optical potential parameters were extracted. Our theoretical analysis on these grounds is described in Sec. III A.

For the microscopic approach we adopted the JLM model according to the code developed by F. S. Dietrich. The model was derived by Jeukenne, Lejeune and Mahaux [1] and was extensively studied for stable nuclei by Mellema *et al.* [13], Hansen *et al.* [14], and Petler *et al.* [15]. It has been particularly successful in describing elastic proton and neutron scattering from medium- and heavy-mass stable nuclei with slight adjustments mainly on the imaginary part of the central potential [36]. The extension of these calculations to light nuclei constitutes a severe test of the applicability of the local-density approximation, which is used to obtain optical potentials for finite nuclei from calculations performed for "infinite nuclear matter." Later, the extension of the model for the drip-line nuclei will be an additional goal. In this direction the application of the JLM model for nuclei with mass from $A = 9$ to 209 [14] seems to provide the appropriate solid working ground for the present work. The applicability also to lower energies than the standard ones where the model is tested [36] ($10 \leqslant E \leqslant 160$ MeV/u) is supported by the work in Ref. [16]. Our theoretical analysis on these grounds is described in Sec. III B. It should be noted that the microscopic approach involves folding procedures, where density distributions are considered explicitly. In this respect, we have been using densities of three different models to be confronted with our present data. Densities of ^{17}O are also used by interchanging proton and neutron distributions for probing mirror symmetry.

We have also focused our analysis on total reaction cross sections. Reaction cross sections are of fundamental interest in nuclear physics, since they provide measurements of the size of nuclei. They are an effective tool for revealing unusual features in nuclei such as extended halos or neutron skins. Therefore, in this study total reaction cross sections have been deduced via our optical potential analysis in both macroscopic and microscopic views, and are compared with values obtained via a standard one-barrier penetration model (Wong [37]), and with the systematics obtained by Kolata and Aguilera [38]. The results are included in Sec. III.

II. EXPERIMENTAL DETAILS

A. Secondary beam

The ^{17}F radioactive beam was produced at the EXOTIC facility [39] at Laboratori Nazionali di Legnaro (LNL-Italy) of the Istituto Nazionale di Fisica Nucleare (INFN) by means of the in-flight technique and by using the reaction $^{1}\mathrm{H}(^{17}\mathrm{O},^{17}\mathrm{F})n$. The $^{17}\mathrm{O}^{+7}$ primary beam was delivered from the LNL-XTU Tandem Van de Graaff accelerator with an intensity of $\sim$70 to 100 pnA and at an energy of 105 MeV. The primary beam was directed to a 5-cm-long gas cell with 2.2-μm-thick Havar foils, filled with H_2 under controlled pressure and temperature conditions. During the experiment the gas pressure and temperature were 990 mbar and $\sim 30\,^{\circ}$C, resulting in an effective thickness of 0.4 mg/cm^2.

The selection, separation, and focusing of the secondary beam was achieved by a quadrapole triplet, a 30°-bending magnet, a 1-m-long Wien filter, and a second quadrupole triplet. Downward across the beam line and 75 cm before the secondary target, one of the two available parallel plate avalanche counters (PPAC_A) was used to improve and monitor the beam spatial profile before and during the measurement. The second PPAC_B of the EXOTIC beam line, placed 21 cm before the target, was nonfunctional. The beam spatial profile at the target position was defined by an appropriate sequence of slits and collimators with a minimum aperture of 12 mm, in a configuration identical with the one described in Ref. [40]. The full width at half maximum (FWHM) of the resulting ^{17}F beam spot at the target position was estimated to be the same as that experimentally deduced in Ref. [40], i.e., $\sim$9 mm in diameter. Beam-purity optimization was achieved by recording the energy spectrum of the secondary beam at different Si detectors placed across the EXOTIC beam line. In Fig. 1 the energy spectrum of the secondary beam can be seen as recorded from the end-channel Si detector placed on the target ladder. In the same figure we see that the only contaminant of the beam is the ^{17}O 16 MeV below the ^{17}F final energy. From the same spectrum we see the result that at higher beam energy the beam purity was better than 98%, whereas at lower energy it was better than 93%. The observed asymmetry of the ^{17}F beam energy distribution as recorded from the end-channel Si detector can be attributed to the initial energy distribution of the ^{17}F secondary beam, which looks like a plateau covering a region of $\sim$15 MeV below the finally selected ^{17}F beam energy [41]. To achieve the optimum ^{17}F beam energy and ion selection, the ion-optical systems mentioned above were

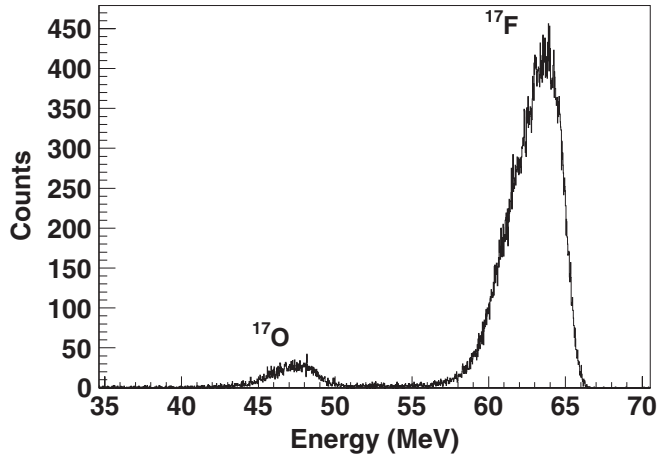

FIG. 1. Energy spectrum of the end-channel detector placed directly on the target ladder. This spectrum corresponds to the lower beam energy (3.5 Mev/u) considered in this work. The ^{17}F secondary beam can clearly be seen together with the main contaminant ^{17}O peak, which accounts for 6.6% of the total beam intensity. For the higher beam energy (4.3 MeV/u) the contamination was smaller than 2%.

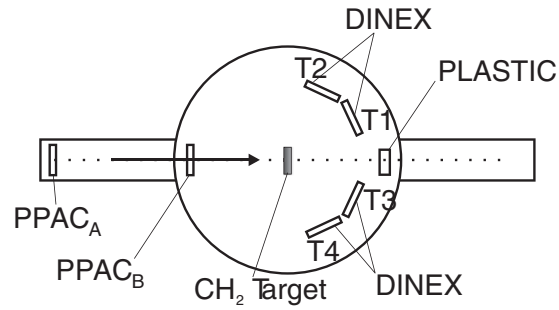

FIG. 2. The experimental setup as realized during the ^{17}F + p experiment. The PPAC$_A$ detector before the scattering chamber, the four DINEX triple-telescopes, as well as the plastic detector can be seen. The PPAC$_B$ detector was not functional.

combined in order to eliminate the low-energy part of the initial energy distribution. Despite the effectiveness of the ion-optical elements, a tiny amount of the low-energy ions remains. Additionally, the separator of the EXOTIC beam line is not fully achromatic—as an ion-optical device with only one dipole magnet—contributing also to the small asymmetry in the final energy distribution of the ^{17}F beam.

The energy of the secondary beam is defined by the primary beam energy as well as by the effective thickness of the primary target. Furthermore, the energy loss of the secondary beam from the different beam line elements on the way to the scattering chamber affects the final energy of the ^{17}F beam. Two beam energies were considered for the present work. For the first run, the energy of the secondary beam was 63.5 ± 1.5 MeV and for the second one it was 77.3 ± 1.4 MeV. The last energy was achieved simply by removing the (nonfunctional) PPAC$_B$ from the beam line. In this way much of the beam time was saved, since it was not needed to retune the EXOTIC facility by changing to another primary beam energy. Additionally, taking into account the energy loss in the 0.93-mg/cm^2 thick CH_2 target results in energies of 3.5 and 4.3 MeV/u at the middle point of the target. In both runs, the secondary beam-energy was chosen to be outside known resonances [23] and was measured before and after each run by the end-channel Si detector. Under these conditions the resulting beam intensity in the secondary target position was $\sim 10^5$ pps.

B. Experimental setup

Elastic scattered protons from the ^{17}F beam on the 0.93-mg/cm^2 thick CH_2 target were detected by means of the DINEX[1] Si-detector array. The DINEX detector array consists of four triple Si telescopes. Each telescope provided three detection stages: (a) $\Delta E_1 = 40$ μm double-sided silicon-strip detector (DSSSD), (b) $\Delta E_2 = 500$ μm silicon pad detector, and (c) $E_{\rm res} = 1000$ μm DSSSD. The four telescopes were placed at 104 mm distances from the target position according to the configuration shown in Fig. 2. With this setup the covering detection area of $4 \times 50 \times 50$ mm^2 corresponds to an overall solid angle of $\sim$0.8 sr. The high laboratory angular coverage ranging between 11° and 85° corresponds to a center-of-mass angular coverage of 10° to 158°. Due to some damaged strips or/and to high electronic noise, the actual angular coverage in the laboratory frame was limited to 11°–65°, resulting in 50°–158° for the center-of-mass frame. As can be seen in Fig. 2, two telescopes of the DINEX array were placed on each side of the scattering chamber in a slightly asymmetrical way. In this way continuous angular-distribution data were collected. Position information was available at the first and the third detection stages of each telescope. For each 16×16 DSSSD detector the position information for each hit was determined from the identification numbers of each of the x and y strips that fired. Considering just the y-strip data, the resulting angular resolution was in the range of 1.3°–3.1° depending on the strip position. In order to reduce the electronic noise in the case of DSSSD, detectors a coincidence between the "OR" of p junctions (y strip) and of the "OR" of n junctions (x strip) for each DSSSD module was required to produce the corresponding gate signal.

Besides the DSSSD detectors, one plastic detector placed at the end cup of the scattering chamber (see Fig. 2) was used for beam-intensity monitoring reasons. The plastic scintillator was placed 220 mm after the target position at 0°, covering the lab angular range of 0°–5°. Elastic scattered ^{17}F ions from the proton target were detected via the plastic detector, together with the nonscattered ions.

The overall trigger condition resulted from a triple coincidence requirement of (a) the total "OR" of all DINEX detectors, (b) a hit at the plastic detector, and (c) a valid signal on the PPAC$_A$ detector. Therefore protons in the DINEX detectors were recorded only if a valid coincidence between PPAC$_A$ detector, the DINEX array, and the plastic detector was registered. In this way, protons originating from reactions of fluorine on carbon were suppressed and the overall dead time

[1]DINEX: DIspersión de Núcleos EXóticos (in English: scattering of exotic nuclei).

due to high counting rate of the beam particles dumped in the plastic detector was decreased. Beam intensity was recorded by using an independent down-scaled trigger signal originating from the plastic scintillator.

C. Data reduction

The first stage of the data analysis procedure was the angular coverage and solid angle determination of each strip of the DSSSD detectors. This was done by extensive GEANT4 [42] Monte Carlo (MC) calculations where all the details of the beam profile, the target, and the detection geometry were taken into account. At the second stage, the deduced results from the MC calculations were combined with the counting rate per strip that resulted from the ^{17}F+^{198}Au run at the sub-Coulomb barrier energy of 72 MeV. At this energy a Rutherford angular distribution was expected. This run proved to be very useful for the solid angle as well as for the overall angular calibration of the DINEX array. The results of the angular calibration procedure—the combination of the gold calibration run and the MC calculations—can be seen in Fig. 3. The agreement of the theoretical angular distribution with the corresponding experimental points visualizes the precision of the angular calibration procedure. In the same figure the angular resolution that was obtained from MC calculations by considering only the p strips of the DINEX detectors can be seen.

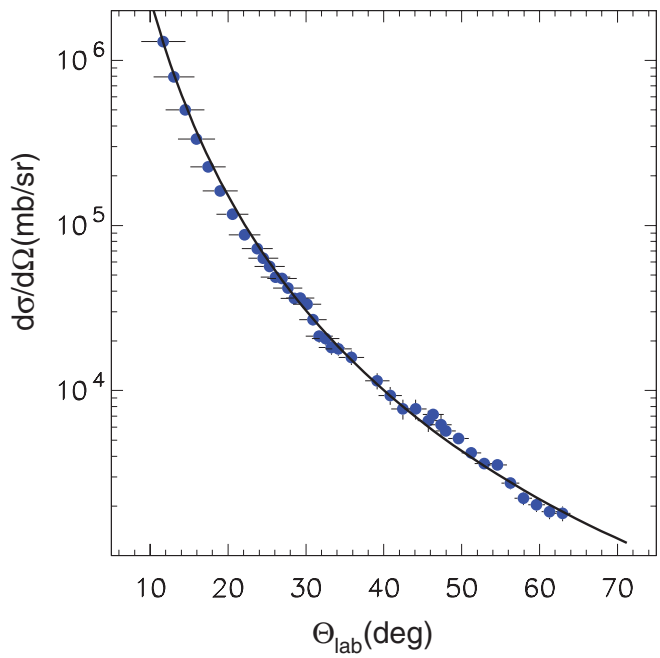

FIG. 3. (Color online) The experimentally deduced angular distribution of the ^{17}F + ^{197}Au calibration run together with the expected Rutherford scattering reaction cross section. The experimental points were deduced by taking into account the angular coverage and the solid angle for each p strip as deduced from MC calculations. The horizontal error bars correspond to the p-strip angular resolution as deduced from MC calculations.

Besides the "hardware" triple coincidence (DINEX$\wedge$PPAC$_A\wedge$Plastic), during the analysis procedure a multiplicity software condition (multiplicity $\leqslant 3$) on the number of hits at the same detection module was applied in order to remove the pulser peak from the region of interest without reducing the number of counts. Some typical p-strip energy spectra can be seen in Fig. 4. The absolute normalization of the experimental data was done according to the work of Harss *et al.* [23].

The overall error for each data point of the deduced angular distributions ranges from 9% up to 27% and originates mainly from statistical uncertainty. Other systematic sources of uncertainty, for instance the uncertainty of the solid angle covered from each strip, target thickness fluctuations, and beam intensity determination errors, were also included. The uncertainty of the absolute normalization of the data according to the work of Harss *et al.* [23] was not included and was estimated to be less than 20%.

III. THEORETICAL ANALYSIS

The elastic scattering data were analyzed using standard phenomenological optical potentials and within the framework of the JLM microscopic model employing nuclear matter calculations using realistic nucleon-nucleon interactions.

A. Macroscopic analysis

For the macroscopic optical model analysis of the elastic scattering data different global parametrizations were used (see Table I) in terms of conventional Woods-Saxon form factors. In Fig. 5 the experimental angular distributions can be seen together with the corresponding theoretical calculations. In all cases the phenomenological analysis of the data in terms of the optical model potential (OMP) was done by means of the ECIS code [35]. As can be seen, no global parametrization is fully compatible with the A, Z, and beam-energy of the present work.

In order to obtain an improved set of OMP parameters for the $^{17}\mathrm{F} + p$ system, the initial values of the seven parametrizations shown in Table I were used as starting points in a grid search, where the depth, radius, and diffuseness of the real part of the potential were fitted one by one to the experimental data, keeping fixed the other two and the

TABLE I. Global OM potentials considered. The E range refers to the incident proton-beam energies (direct kinematics).

Name	Ref.	Z range	A range	E range (MeV)
Menet	[8]	6–82	12–208	30.0–60.0
Madland	[9]	6–82 f	12–208	50.0–400.0
Koning	[10]	13–83	27–209	0.0–200.0
Becchetti	[3]	20–83	40–209	10.0–50.0
Xiaohua	[11]	12–94	24–240	0.0–200.0
Varner	[4]	20–83	40–209	16.0–65.0
Watson	[9]	3–8	6–16	10.0–50.0

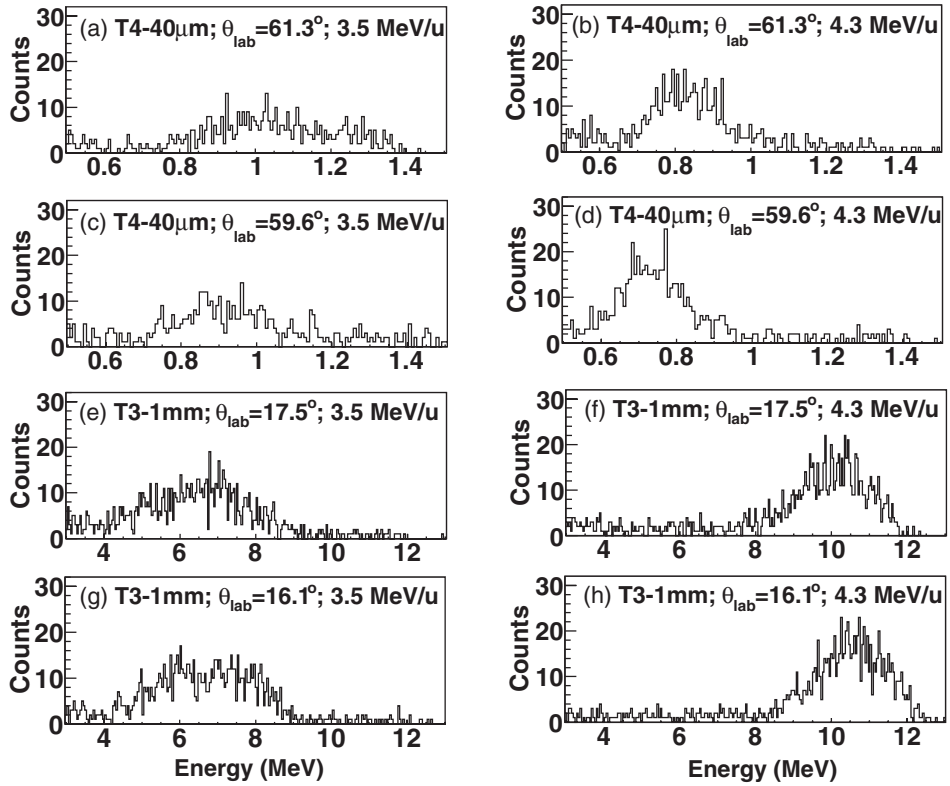

FIG. 4. Some p-strip energy spectra. The left column [spectra (a), (c), (e), and (g)] corresponds to the lower beam energy of 3.5 MeV/u and the right one [spectra (b), (d), (f), and (h)] to 4.3 MeV/u. The upper spectra (a)–(d) for each energy are results from two sequential strips (6 and 7) of the $\Delta E_1 = 40$ μm detection stage of the T4 telescope. The two lower rows of spectra (e)–(h) are results from the T3 telescope from the $E_{\rm res} = 1000$ μm stage (strips 10 and 11).

imaginary part of the potential. Afterwards, a similar scan was tried for the imaginary part of the potential. It was found that the fit was not sensitive to changes of the imaginary potential and for this reason the global parametrization values were adopted for the imaginary part. The best results obtained, from the seven parametrizations shown in Table I, are those produced with the potential parameters from Watson [7] and Xiaohua [11] . The best-fit parameters for the depth (V_R), the radius (r_v), and the diffuseness (a_v) are given in Table II, in addition to the rest of the parameters that were not fitted to the experimental data. In Fig. 6 the experimentally deduced angular distributions are compared with the calculations shown above. Both in Table II as well as in Fig. 6, the deduced OM potentials from the fitting procedure described above are named as "Watson" and "Xiaohua," indicating only the initial parametrizations.

It should be noted that, due to our experimental setup, especially the target thickness, the inelastic excitation to the first excited state of ^{17}F ($E = 495$ keV) was not resolved in this experiment, and the elastic scattering data include also the inelastic excitation. Taking into account in our calculations inelastic coupling, and extracting the level deformation from the reduced matrix element $B(E_2 : 5/2^+ \rightarrow 1/2^+) = 21.67\, e^2\text{fm}^4$ [43], we conclude that this excitation (see Table II) does not exceed 8%.

B. Microscopic analysis

JLM microscopic calculations were performed in a microscopic distorted wave Born approximation (DWBA) approach, in which entrance- and exit-channel optical potentials are calculated consistently using an energy- and density-dependent interaction. This interaction was derived from the nuclear matter calculations of Jeukenne, Lejeune, and Maxaux [1]. The starting points for computing the JLM potentials are the Brueckner-Hartree-Fock (BHF) approximation and the Reid hard-core nucleon-nucleon interaction, which provides, for energies up to 160 MeV, the energy and density dependence of the isoscalar, isovector, and Coulomb components of the complex optical potential in infinite matter. The optical potential of a finite nucleus is obtained by making the local density approximation (LDA), which substitutes the nuclear matter density with the density distribution of the nucleus, and by including the effect of the range of the effective interaction in a phenomenological way [36]. As was pointed out in the introduction, the present analysis provides a severe test of this approximation, as the projectile nucleus (inverse kinematics proton elastic scattering) has a low mass number.

Initially JLM elastic scattering calculations were performed in a standard normalization ($\lambda_v = 1.0$ and $\lambda_w = 0.8$). Proton and neutron density distributions were calculated according to three models.

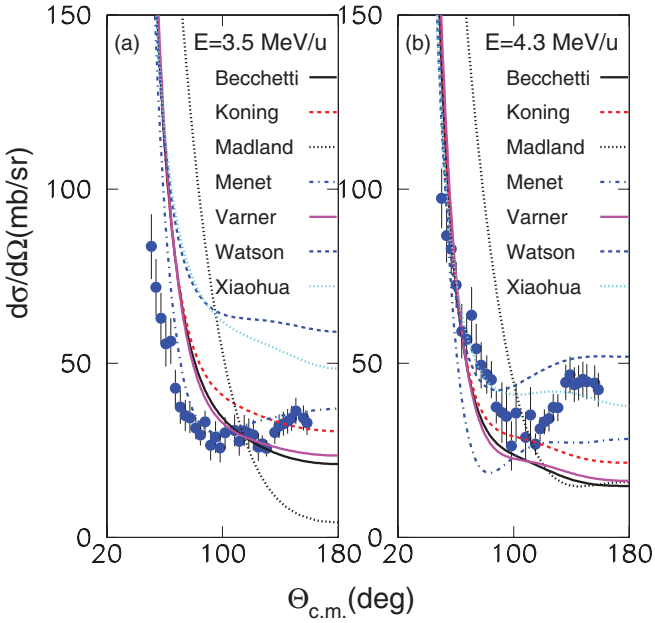

FIG. 5. (Color online) Angular distribution calculations adopting seven global proton-nucleus potentials (Refs. [3,4,7–11]) are presented together with the experimental data at 3.5 MeV/u (a) and 4.3 MeV/u (b). The presented calculations do not include any kind of fit to the experimental data.

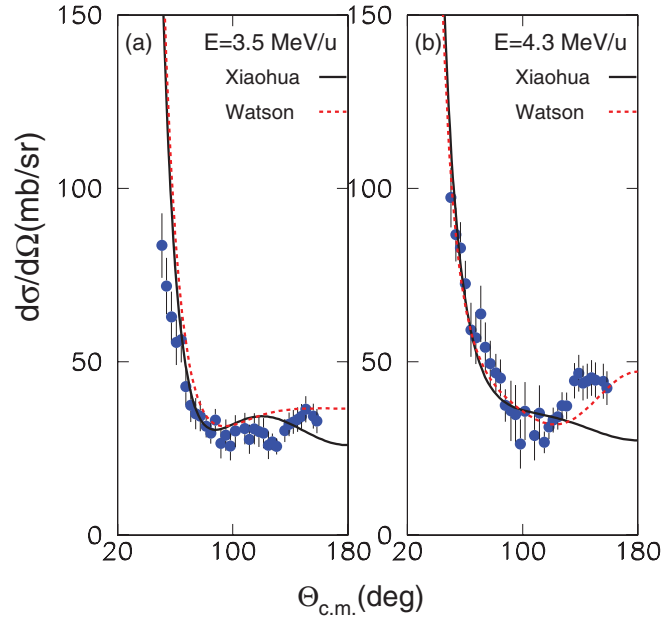

FIG. 6. (Color online) From the different global parametrizations used as a starting values in the fitting procedure described in Sec. III A, those that better reproduce the experimental results are presented here, together with the experimental data at both energies: 3.5 MeV/u (a) and 4.3 MeV/u (b). The potential parameters of both Watson [7] and Xiaohua [11] are given in Table II.

In one approach we considered a cluster model, the Neo-COSM model as developed by Masui, Kato, and Ikeda [44,45]. In this model the complex scaling method (CSM) [46] is applied to the cluster orbital shell model (COSM) formalism [47]. Resonant and bound states are considered in the same framework. The core dynamics are introduced via a core-size parameter.

In a second approach, the relativistic Hartree-Bogoliubov (RHB) model [48] is considered. This model provides an excellent description of ground state and excited states in nuclei at and far away from stability in a unified description of mean-field and pairing correlations. The Lagrangian parameter set DD-ME2 is used [49]. This set has an explicit density dependence on both isoscalar and isovector channels and the finite-range pairing force D1S of Gogny [50].

In a third approach we have used the simpler nonrelativistic Hartree-Fock (HF) model, with the parametrization SGII for the Skyrme interaction, within the filling approximation (we assume that the last proton fills by one sixth the $d_{5/2}$ shell).

The JLM results with the three densities are shown in Fig. 7 for 4.3 and 3.5 MeV/u. For the higher energy of 4.3 MeV/u, the agreement of the calculation with the data, at least for the last two approaches, is remarkable. This indicates that the LDA approximation holds even for a light nucleus such as ^{17}F, and moreover that it holds for near-barrier energies ($E = 2.3V_{\rm bar}$). The obvious disagreement at the lower energy of 3.5 MeV/u, if not related to experimental problems of the overall normalization, is interesting and should be further explored.

The densities that seem to reproduce the data better are the ones calculated via a RHB theory with the DD-ME2 interaction and via HF theory using SGII for the Skyrme interaction. These two models are slightly different at higher energies, where the data cannot give a definitive precedence. An attempt was made to test symmetry between the two mirror nuclei ^{17}F and ^{17}O. For that we have been using the experimental density distribution of oxygen represented by a HO shape [51], interchanging the proton and neutron densities (the neutron density for oxygen was taken as $\rho_n = N/Z\rho_p$). The results describe equally well the data as the other calculations, and indeed are almost identical with the ones obtained via the simpler HF-SGII calculation. The symmetry of the neutron and proton distribution is not however a surprising issue, since the isospin mixing for this light nucleus is expected to be minimal [52], producing small energy shifts between the proton and neutron single-particle levels, with an even smaller effect on the radial shapes of the single-particle wave functions and thus on the density. A proton skin structure for the ^{17}F nucleus, with a small difference in the tail of the proton density distribution due to the contribution by the last weakly bound ($1d_{5/2}$) proton, cannot be easily traced in this interchange between proton and neutron densities via the elastic scattering distribution data.

The above analysis, while very effectively probing the adequacy of the JLM microscopic calculation in a low mass and energy region, cannot differentiate between the various densities. In that respect this analysis shows that the static part of the potential does not depend so much on the vicinity of the drip lines. Especially in the mean-field scheme, most of the particles are well bound and they give almost the total contribution to the density, while the last proton producing the longer tail gives very little effect. On the other hand a strong effect can be only observed on the dynamical or polarization part of the potential, and this can be probed

TABLE II. Optical-model potentials obtained for ^{17}F + p, and the corresponding calculated total reaction and inelastic scattering cross sections to the first excited state of ^{17}F. In all cases standard Woods-Saxon form factors were considered. In this table the modified Watson [7] and Xiaohua [11] global parametrizations are given, which better reproduced the experimentally deduced angular distributions by fitting the depth, radius, and diffuseness of the real part of each potential. The rest of the parameters are the same as those resulting from the global parametrizations, scaled to the mass and energy of the present work. The depths of the different potential components are in MeV, the radius and diffuseness parameters are in fm, and the cross sections are in mb.

	3.5 MeV/u		4.3 MeV/u	
	Watson	Xiaohua	Watson	Xiaohua
V	54.4	47.7	59.4	53.5
r_V	1.15	1.16	1.15	1.16
a_V	0.57	0.6	0.57	0.6
W	–	0.04	–	0.06
r_W	–	1.16	–	1.16
a_W	–	0.6	–	0.6
V_s	–	3.01	–	3.2
r_{Vs}	–	1.17	–	1.17
$a_V s$	–	0.72	–	0.72
W_s	2.15	1.92	2.65	2.33
r_{Ws}	1.15	1.17	1.15	1.17
a_{Ws}	0.50	0.72	0.5	0.72
V_{so}	5.5	8.21	5.5	8.18
r_{so}	1.15	1.17	1.15	1.17
a_{so}	0.57	0.72	0.57	0.72
r_C	1.25	1.1	1.25	1.1
σ_r	414	466	523	543
σ_{inel}	27.0	22.4	43.6	24.6

by, e.g., inelastic scattering, hidden in this work due to the particular experimental conditions.

Best-fit normalization factors are presented in Table III, while the results of the best fits are shown in Fig. 8. It can be seen that the results for the higher energy are close to the standard values, while for the lower energy the real part has to be substantially reduced.

A substantial contribution of this work relies also on the extraction of total reaction cross-sections. Results of the total reaction cross sections, deduced from the best fits, are included in Table IV. For the microscopic approach an error analysis of the best fits was applied, and the appropriate errors to the

TABLE III. Best-fit normalization factors for the real, λ_v, and imaginary, λ_w, terms of the JLM potential with three densities: Neo-COSM, HB-DDME2, and HF-SGII.

Norm	3.5 MeV/u	4.3 MeV/u
λ_v	0.80 ± 0.14	0.93 ± 0.08
	0.85 ± 0.02	0.99 ± 0.02
	0.86 ± 0.02	0.90 ± 0.02
λ_w	0.75 ± 0.11	0.86 ± 0.08
	0.73 ± 0.10	0.65 ± 0.06
	0.66 ± 0.09	0.66 ± 0.06

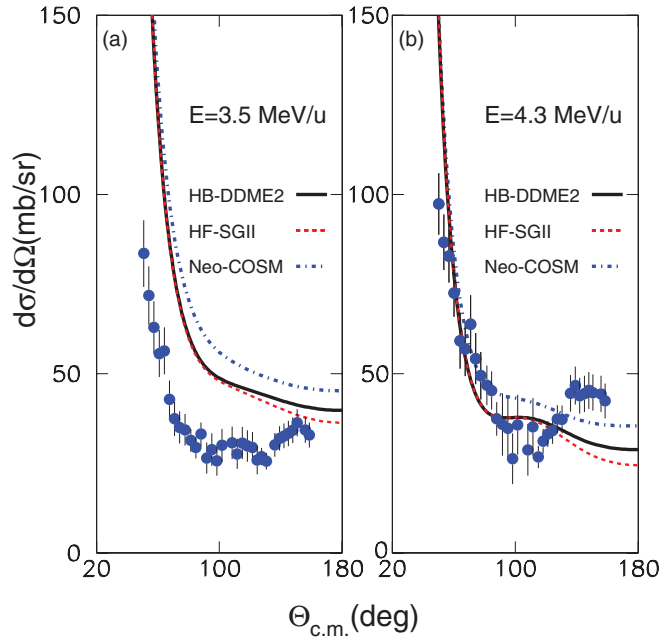

FIG. 7. (Color online) Elastic scattering ^{17}F + p data at both beam energies (3.5 MeV/u and 4.3 MeV/u). The lines represent JLM calculations with standard normalization factors $\lambda_v = 1.0$ and $\lambda_w = 0.8$, taking into account density distributions via a Neo-COSM model, HF with Skyrme interaction, and relativistic mean field with HB and DDME2 interaction.

two fitted normalization factors for the real and imaginary terms were assigned. Subsequently the uncertainties to the cross sections were deduced as follows. Keeping one of the normalization factors constant to the best value and by using

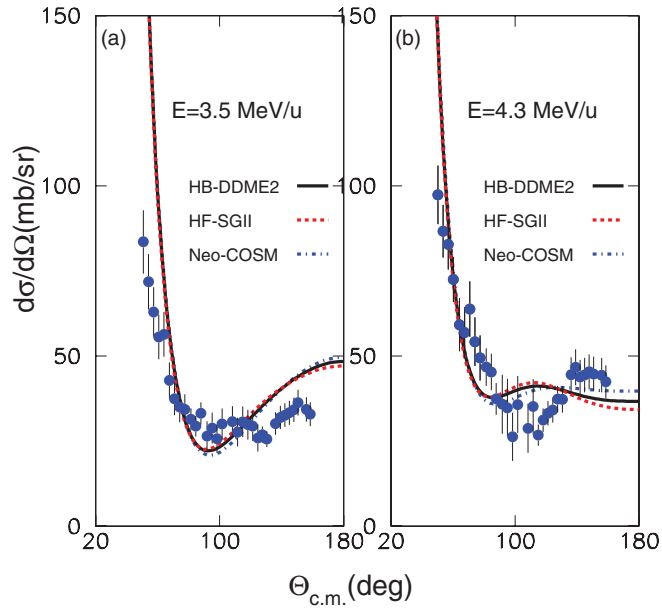

FIG. 8. (Color online) Elastic scattering ^{17}F + p data at both beam energies (3.5 MeV/u and 4.3 MeV/u). The lines represent JLM calculations with best-fit normalization factors λ_v and λ_w, taking into account density distributions via a Neo-COSM model, HF with Skyrme interaction, and relativistic mean field with HB and DDME2 interaction.

TABLE IV. Total reaction cross section σ_{Wong} according to the Wong one-barrier penetration model, and cross sections σ_W and σ_X according to our fit procedures, adopting the Watson and Xiaohua phenomenological potentials respectively, but varying, for a better fit, the volume, radius, and absorption of the real central part. Also shown are cross sections according to our microscopic JLM approach with best-fit normalization factors appearing in Table III, for three densities according to Neo-COSM (σ_{jlm1}), HB-DDME2 (σ_{jlm2}), and HF-SgII (σ_{jlm3}) interactions.

E_{beam} (MeV/u)	σ_{Wong} (mb)	σ_W (mb)	σ_X (mb)	σ_{jlm1} (mb)	σ_{jlm2} (mb)	σ_{jlm3} (mb)
3.5	325	414 ± 37	466 ± 42	510 ± 6	550 ± 10	569 ± 10
4.3	405	523 ± 89	543 ± 92	538 ± 11	535 ± 10	543 ± 13

the upper or/and the lower limit of the other as the second normalization factor, cross sections were estimated and vice versa. This procedure was not applicable for the macroscopic approach, where more than two parameters were fitted. To get an estimation of the sensitivity of the extracted reaction cross sections from the macroscopic calculations, the following procedure was applied: The experimental data were shifted to the maximum and/or to the minimum values of their error bars, and different best fits were tried according to the previously described procedure. The different values of reaction cross sections deduced from the modified experimental data were used for the corresponding uncertainty estimations given in Table IV. In the same table, results of the one-barrier penetration model calculation are also included, as well as results of the phenomenological approach, described in the previous section. It can be seen that the obtained cross sections are 20% to 30% larger than standard values, indicating an unusual structure for this drip-line neutron-deficient nucleus. Taking into account that the adopted theoretical density distributions for the ground state refer to a proton skin rather than a halo structure, with some caution we could suggest and support this idea in agreement with previous works [30–33]. Further, our reaction cross sections are consistent with the global results obtained by Kolata and Aguilera [38] and by Gomes *et al.* [53] for weakly bound but nonhalo nuclei.

IV. CONCLUSIONS

Elastic scattering angular distributions for the reaction $^{17}\text{F} + p$ were measured at two near-barrier energies, 3.5 and 4.3 MeV/u. The results were analyzed via phenomenological as well as microscopic models for probing the optical potential. It was shown that global parametrizations fail to reproduce the experimental results. On the other hand the superiority of the microscopic approach via JLM calculations was demonstrated at least for the higher energy. In this respect the adequacy of the LDA approximation for a light nucleus such as ^{17}F it was shown, and the energy range extension of this description to the low energy of 4.3 MeV/u was validated. Total reaction cross sections were extracted from both modes of analysis, macroscopic and microscopic, after a best-fit analysis and were found to be consistent. The obtained values were compared with Wong's estimates and were found to be larger by at least 23%. Taking into account the density distributions used in the microscopic analysis and global predictions for weakly bound nonhalo nuclei, we conclude that the ground state of the ^{17}F nucleus presents rather a proton skin structure and not a halo one, in accordance with most of the previous findings.

ACKNOWLEDGMENTS

We warmly thank all the operators of the LNL-XTU Tandem Van de Graaff accelerator for the excellent beam conditions of the provided ^{17}O primary beam over the whole duration of the experiment. This work has been partially supported by the Italian M.I.U.R. within Project No. RBFR08P1W2_001 (FIRB 2008) and the Spanish Ministerio de Ciencia e Innovación under Project No. FPA2010-22131-C02-01.

[1] J. P. Jeukenne, A. Lejeune, and C. Mahaux, Phys. Rev. C **16**, 80 (1977).
[2] F. A. Brieva and J. R. Rook, Nucl. Phys. A **307**, 493 (1978).
[3] F. D. Becchetti and G. W. Greenlees, Phys. Rev. **182**, 1190 (1969).
[4] R. L. Varner, W. J. Thompson, T. L. McAbee, E. J. Ludwig, and T. B. Clegg, Phys. Rep. **201**, 57 (1991).
[5] E. D. Cooper, S. Hama, B. C. Clark, and R. L. Mercer, Phys. Rev. C **47**, 297 (1993).
[6] S. Hama, B. C. Clark, E. D. Cooper, H. S. Sherif, and R. L. Mercer, Phys. Rev. C **41**, 2737 (1990).
[7] B. A. Watson, P. P. Singh, and R. E. Segel, Phys. Rev. **182**, 977 (1969).
[8] J. J. H. Menet, E. E. Gross, J. J. Malanify, and A. Zucker, Phys. Rev. C **4**, 1114 (1971).
[9] D. G. Madland, in Proceedings of OECD/NEA Specialists Meeting on Nucleon-Nucleus Optical Model to 200 MeV, 1997, p. 129 (unpublished); this can also be found as arXiv:nucl-th/9702035v1.
[10] A. J. Koning and J. P. Delaroche, Nucl. Phys. A **713**, 231 (2003).
[11] Xiaohua Li and Chonghai Cai, Nucl. Phys. A **801**, 43 (2008).
[12] F. Petrovich, S. K. Yoon, M. J. Threapleton, R. J. Philpott, J. A. Carr, F. S. Dietrich, and L. F. Hansen, Nucl. Phys. A **563**, 387 (1993).
[13] S. Mellema, R. W. Finlay, F. S. Dietrich, and F. Petrovich, Phys. Rev. C **28**, 2267 (1983).
[14] L. F. Hansen, F. S. Dietrich, B. A. Pohl, C. H. Poppe, and C. Wong, Phys. Rev. C **31**, 111 (1985).

[15] J. S. Petler, M. S. Islam, R. W. Finlay, and F. S. Dietrich, Phys. Rev. C **32**, 673 (1985).
[16] F. S. Dietrich, R. W. Finlay, S. Mellema, G. Randers-Pehrson, and F. Petrovich, Phys. Rev. Lett. **51**, 1629 (1983).
[17] G. R. Satchler, Phys. Rep. **199**, 147 (1991).
[18] N. Alamanos, A. Pakou, A. Lagoyannis, and A. Musumarra, Nucl. Phys. A **660**, 406 (1999).
[19] A. Pakou N. Alamanos, P. Roussel-Chomaz, F. Auger, D. Rosengrant, and A. de Vismes, Nucl. Phys. A **691**, 661 (2001).
[20] N. Alamanos, F. Auger, B. A. Brown, and A. Pakou, J. Phys. G **24**, 541 (1998).
[21] A. de Vismes, P. Roussel-Chomaz, W. Mittig, A. Pakou, N. Alamanos, F. Auger, J.-C. Angélique, J. Barrette, A. V. Belozyorov, C. Borcea *et al*., Phys. Lett. B **505**, 15 (2001).
[22] R. Wolski, A. Pakou, and N. Alamanos, Yad. Fiz. **65**, 769 (2002) [Phys. At. Nucl. **65**, 736 (2002)].
[23] B. Harss, C. L. Jiang, K. E. Rehm, J. P. Schiffer, J. Caggiano, P. Collon, J. P. Greene, D. Henderson, A. Heinz, R. V. F. Janssens *et al*., Phys. Rev. C **65**, 035803 (2002).
[24] M. Dufour and P. Descouvemont, Nucl. Phys. A **730**, 316 (2004).
[25] R. Morlock, R. Kunz, A. Mayer, M. Jaeger, A. Müller, J. W. Hammer, P. Mohr, H. Oberhummer, G. Staudt, and V. Kölle, Phys. Rev. Lett. **79**, 3837 (1997).
[26] K. Riisager, A. S. Jensen, and P. Moller, Nucl. Phys. A **548**, 393 (1992).
[27] H. Kitagawa and H. Sagawa, Phys. Lett. B **299**, 1 (1993).
[28] Zhongzhou Ren, Amand Faessler, and A. Bobyk, Phys. Rev. C **57**, 2752 (1998).
[29] Z. Ren and A. Faessler, J. Phys. G: Nucl. Part. Phys. **24**, 1823 (1998).
[30] A. Ozawa, T. Kobayashi, H. Sato, D. Hirata, I. Tanihata, O. Yamakawa, K. Omata, K. Sugimoto, D. Olson, W. Christie, and H. Wieman, Phys. Lett. B **334**, 18 (1994).
[31] H. Y. Zhang, W. Q. Shen, Z. Z. Ren, Y. G. Ma, W. Z. Jiang, Z. Y. Zhu, X. Z. Cai, D. Q. Fang, C. Zhong, L. P. Yu *et al*., Nucl. Phys. A **707**, 303 (2002).
[32] M. Romoli, E. Vardaci, M. Di Pietro, A. De Francesco, A. De Rosa, G. Inglima, M. La Commara, B. Martin, D. Pierroutsakou, M. Sandoli *et al*., Phys. Rev. C **69**, 064614 (2004).
[33] Z. Dongmei, Z. Yongnan, Y. Daqing, Z. Xizhen, Z. Yi, T. Minamisono, M. Matsuta, M. Fukuda, M. Mihara, Z. Chunlei *et al*., J. Phys. G: Nucl. Part. Phys. **34**, 523 (2007).
[34] R. Lewis and A. C. Hayes, Phys. Rev. C **59**, 1211 (1999).
[35] J. Raynal, Phys. Rev. C **23**, 2571 (1981).
[36] N. Alamanos and P. Roussel-Chomaz, Ann. Phys. Fr. **21**, 601 (1996).
[37] C. Y. Wong, Phys. Rev. Lett. **31**, 766 (1973).
[38] J. J. Kolata and E. F. Aguilera, Phys. Rev. C **79**, 027603 (2009).
[39] F. Farinon, T. Glodariu, M. Mazzocco, A. Battistella, R. Bonetti, L. Costa, A. De Rosa, A. Guglielmetti, G. Inglima, M. La Commara *et al*., Nucl. Instrum. Methods Phys. Res., Sect. B **266**, 4097 (2008).
[40] M. Mazzocco, C. Signorini, D. Pierroutsakou, T. Glodariu, A. Boiano, C. Boiano, F. Farinon, P. Figuera, D. Filipescu, L. Fortunato *et al*., Phys. Rev. C **82**, 054604 (2010).
[41] M. Mazzocco, F. Farinon, T. Glodariu, H. Geissel, A. Guglielmetti, N. Iwasa, M. La Commara, B. Martin, C. Mazzocchi, D. Pierroutsakou *et al*., Nucl. Instrum. Methods. Phys. Res., Sect. B **266**, 4665 (2008).
[42] S. Agostinelli, J. Allison, K. Amako, J. Apostolakis, H. Araujo, P. Arce, M. Asai, D. Axen, S. Banerjee, l, G. Barrand *et al*., Nucl. Instrum. Methods Phys. Res., Sect. A **506**, 250 (2003).
[43] D. R. Tilley, H. R. Weller, and C. M. Cheves, Nucl. Phys. A **564**, 1 (1993).
[44] H. Masui, K. Kato, and K. Ikeda, Phys. Rev. C **73**, 034318 (2006).
[45] H. Masui, private communication.
[46] J. Anguilar and J. M. Combes, Commun. Math. Phys. **22**, 269 (1971); E. Balslev and J. M. Combes, *ibid*. **22**, 280 (1971); Y. K. Ho, Phys. Rep. **99**, 1 (1983).
[47] S. Aoyama, S. Mukai, K. Klato, and K. Ikeda, Prog. Theor. Phys. **93**, 99 (1995).
[48] D. Vretenar, A. V. Afanasjev, G. A. Lalazissis, and P. Ring, Phys. Rep. **409**, 101 (2005).
[49] G. A. Lalazissis, T. Niksic, D. Vretenar, and P. Ring, Phys. Rev. C **71**, 024312 (2005).
[50] J. F. Berger, M. Girod, and D. Gogny, Nucl. Phys. A **428**, 23c (1984).
[51] H. De Vries, C. W. De Jager and C. E. vries, At. Data Nucl. Data Tables **36**, 495 (1987).
[52] G. Colo, M. A. Nagarajan, P. Van Isacker, and A. Vitturi, Phys. Rev. C **52**, R1175 (1995); and private communication.
[53] P. R. S. Gomes, J. Lubian, I. Padron, and R. M. Anjos, Phys. Rev. C **71**, 017601 (2005).